Towards Robust Designs Via Multiple-Objective Optimization Methods

Man Mohan Rai*
NASA Ames Research Center, Moffett Field, CA-94035, USA

INTRODUCTION

Fabricating and operating complex systems involves dealing with uncertainty in the relevant variables. In the case of aircraft, flow conditions are subject to change during operation. Efficiency and engine noise may be different from the expected values because of manufacturing tolerances and normal wear and tear. Engine components may have a shorter life than expected because of manufacturing tolerances. In spite of the important effect of operating- and manufacturing-uncertainty on the performance and expected life of the component or system, traditional aerodynamic shape optimization has focused on obtaining the best design given a set of deterministic flow conditions. Clearly it is important to both maintain near-optimal performance levels at off-design operating conditions, and, ensure that performance does not degrade appreciably when the component shape differs from the optimal shape because of manufacturing tolerances and normal wear and tear. These requirements naturally lead to the idea of robust optimal design wherein the concept of robustness to various perturbations is built into the design optimization procedure.

Recognition of the importance of incorporating the probabilistic nature of the variables involved in designing and operating complex systems has led to several investigations in the recent past. Some of the basic principles of robust optimal design are discussed by Egorov et al.[1]. Several commonly used approaches such as maximizing the mean value of the performance metric, minimizing the deviation of this metric and, maximizing the probability that the efficiency value is no less than a prescribed value are discussed in their paper. Egorov et al.[1] make the observations that a) robust design optimization is in essence multi-objective design optimization because of the presence of the additional objective (robustness) and, b) the addition of the robustness criterion may result in an optimal solution that is substantially different from that obtained without this criterion. Various approaches to robust optimal design are also mentioned in this article.

While the discussion above focused on the effect of uncertainty in the variables on performance, their effect on constraint satisfaction is equally important from a reliability perspective. Here the focus is on maximizing the probability of constraint satisfaction. Koch et al.[2], provide a discussion of this and related concepts. Some of the basic steps involved in both robust optimal design as well as reliability-based optimization such as a) identifying random variables and their associated probability density functions, b) reducing this set of variables to a smaller subset of key random variables, to reduce optimization costs and, c) the effective utilization of Monte Carlo techniques to obtain estimates of performance variability or reliability, are discussed by the authors.

Simulation based design optimization can be computationally expensive in cases where the underlying physics is complicated. Some of the contributing factors are three-dimensionality, a large disparity in the largest and smallest scales that are required for an accurate analysis etc. The addition of the robustness criterion can greatly increase computational requirements because of the need to estimate the variance in performance or reliability. Koch et al.[2], reduce computational cost by first obtaining the optimal solution via a deterministic approach and subsequently adding the reliability requirement. In a separate article Koch et al.[3]use Kriging models to compute performance variability and reliability.

The imposition of the additional requirement of robustness results in a multiple-objective optimization problem requiring appropriate solution procedures. Typically the costs associated with

*Senior Scientist, Exploration Technology Directorate

multiple-objective optimization are substantial. Therefore efficient multiple-objective optimization procedures are crucial to the rapid deployment of the principles of robust design in industry. Hence the companion set of lecture notes (Single- and Multiple-Objective Optimization with Differential Evolution and Neural Networks [4]) deals with methodology for solving multiple-objective optimization problems efficiently, reliably and with little user intervention.

Genetic and evolutionary algorithms have been applied to solve numerous problems in engineering design where they have been used primarily as optimization procedures. These methods have an advantage over conventional gradient-based search procedures because they are capable of finding global optima of multi-modal functions (not guaranteed) and searching design spaces with disjoint feasible regions. They are also robust in the presence of noisy data. Another desirable feature of these methods is that they can efficiently use distributed and parallel computing resources since multiple function evaluations (flow simulations in aerodynamics design) can be performed simultaneously and independently on multiple processors. For these reasons genetic and evolutionary algorithms are being used more frequently in design optimization. Deb[5] reviews numerous genetic and evolutionary algorithms for use in multiple-objective optimization. More recent developments such as 1) using hierarchical population topologies, 2) surrogate models to compute the objective function, 3) clustering of data into multiple classes for improved algorithm performance and constructing multiple response surfaces and 4) using non-dominated solutions from previous generations, can be found in Refs.6 - 8.

Here we focus on applications of an evolutionary algorithm for multiple-objective optimization developed by Rai.[9] This method is based on the method of Differential Evolution (DE) developed by Price and Storn[10] for single-objective optimization. One goal of this developmental effort was a method that required a small population of parameter vectors to solve complex multiple-objective problems involving several Pareto fronts (global and local) and nonlinear constraints. Applications of this evolutionary method to some difficult model problems involving the complexities mentioned above are also presented in Ref.9. The computed Pareto-optimal solutions closely approximate the global Pareto-front and exhibit good solution diversity. Many of these solutions were obtained with relatively small population sizes. Rai[9] also explores the possibility of using neural networks to obtain estimates of the Pareto optimal front. Achieving solution diversity and accurate convergence to the exact Pareto front usually requires a significant computational effort with the evolutionary algorithm. The use of neural network estimators has the potential advantage of reducing or eliminating this effort thus reducing cost to design. The estimating curve or surface can be used to generate any desired distribution of Pareto optimal solutions. This method is discussed in detail in the companion set of lecture notes[4].

Applications of this new method[9] to robust design are presented here. The evolutionary method is first used to solve a relatively difficult problem in extended surface heat transfer wherein optimal fin geometries are obtained for different safe operating base temperatures. The objective of maximizing the safe operating base temperature range is in direct conflict with the objective of maximizing fin heat transfer. This problem is a good example of achieving robustness in the context of changing operating conditions. The evolutionary method is then used to design a turbine airfoil; the two objectives being reduced sensitivity of the pressure distribution to small changes in the airfoil shape and the maximization of the trailing edge wedge angle with the consequent increase in airfoil thickness and strength. This is a relevant example of achieving robustness to manufacturing tolerances and wear and tear in the presence of other objectives.

ROBUST DESIGN OPTIMIZATION OF FINS

Extended surface heat transfer, i.e., heat transfer with the aid of fins of different shapes, is of importance in a multitude of engineering applications ranging from transport vehicles, to electronic components, industrial heat exchangers and nuclear power generation. Design optimization in the context of fins deals with reducing fin weight and volume for a given heat load, subject to constraints related to fin shape and size.

Fins used in boiling heat transfer are particularly difficult to analyze from first principles because of the complex flow physics involved. Haley and Westwater[11] and Westwater[12] provide an excellent description of fins used in boiling heat transfer and the associated heat transfer processes. Their experiments show that different types of boiling including nucleate- and transition-boiling, and film boiling occur on these fins. Often, all these boiling modes together with free-convection co-exist at a single operating point resulting in heat transfer coefficients that vary considerably along the length of the fin. Methods of analysis must take these variations in heat transfer coefficient into account to yield accurate estimates of heat load. At low fin-base temperatures (compared to the fluid boiling temperature) the entire fin is in a free-convection mode. As the base temperature increases above the boiling temperature of the fluid, high heat transfer nucleate-boiling appears at the base of the fin. As the temperature is increased further, relatively low heat transfer film boiling appears at the base, followed by high heat transfer transition- and nucleate-boiling further away from the base, and free-convection at the tip of the fin. Additional increases in base temperature result in transition- and nucleate-boiling at the tip of the fin leaving the rest of the fin in a film-boiling mode. Even larger base temperatures result in the entire fin being in a film-boiling mode.

Haley and Westwater[11] and Westwater[12] provide experimental and computational data (temperature profiles and heat load at different base temperatures) for different fin-shapes. The main thrust of these articles is the optimization of the shape of the fin to achieve maximum heat load for a given fin volume, that is, single-objective optimization. Optimizing the performance of fins used in boiling heat transfer requires that the cross-section of the fin be tailored so that most of the surface area is in a nucleate- or transition-boiling mode. Considerable increases in heat load, compared to the heat loads that can be obtained with simple cylindrical spines and rectangular fins, can be achieved by using the optimal cross-sectional area distribution. These optimal shapes are typically complex and are difficult to manufacture. Additionally, as the nucleate- and transition-boiling regimes are pushed off the tip of the fin as the base temperature increases, there can be a sudden and large decrease in the heat load. This phenomenon is undesirable because it occurs just when a higher heat load capacity is required. Here we investigate the possibility of maximizing both the heat load and the safe operating base temperature range (SOBTR) using the multi-objective version of DE[4, 9].

For the sake of simplicity, and without loss in generality, the fin shapes investigated in this optimization study are restricted to double cones with a cylindrical base. Figure 1 shows a schematic of the fin. It is defined using four variables, the length and diameter of the cylindrical base, and the base diameter and length of the truncated cone. The length of the second cone is obtained from a fin-volume constraint. Westwater[12] first suggested this particular geometry as an approximation to an optimal “turnip” shape and conducted an experimental investigation of its efficiency. Rai and Rangarajan[13] provide detailed two-dimensional (axi-symmetric) finite element computations for this fin-shape.

Figure 2 shows the fin heat load as the base temperature is increased. The heat load increases to a maximum value and then abruptly decreases. Optimizing the fin shape (for a given base temperature), to maximize heat load, would yield a fin that would operate close to the peak of the heat load curve. This is undesirable because small increases in operating base temperature result in large decreases in the amount of heat that the fin transfers to the fluid. Figure 3 shows the temperature distribution along the length of the fin. The rapid decrease in temperature in the first 10% of the fin occurs because of the small diameter of the cylindrical base. Thereafter, the temperature drop is more gradual because of the larger cross-sectional area. Assuming that the base temperature is higher than the temperature at which film-boiling occurs, it is clear that the narrow base of the fin can be used to drop the temperature such that the remaining large portion of the fin surface is at a temperature at which nucleate- and transition-boiling occur.

The goal of the multiple-objective optimization is

$$\begin{aligned} &\text{Maximize : Heat Load} = -\left(kA\frac{dT}{dx}\right)_{base} \\ &\text{Maximize : SOBTR} = T_{peak\text{-}heat\text{-}load} - T_{base} \\ &\text{Subject to: Fin Volume} = \text{Constant} \end{aligned} \qquad (1)$$

where k is the thermal conductivity of the fin, A is the cross-sectional area of the fin at its base, dt/dx is the temperature gradient at the base, T_{base} is the base temperature and $T_{peak\text{-}heat\text{-}load}$ is the base temperature at which the peak heat load is obtained for a given shape. The base temperature and the fluid temperature were specified as 320 $^{\circ}$F and 120 $^{\circ}$F, respectively. The temperature variation in the fin was computed by solving the one-dimensional heat conduction equation using an iterative finite-difference method.

Ten parameter vectors were used in the optimization and the evolutionary process was run for 80 generations. This required computing 29592 temperature distributions, which far exceeds the 800 (80x10) simulations that would normally be required. This is because the accurate evaluation of the SOBTR for each fin-shape requires numerous temperature-distribution computations (each with a different base temperature). Figure 4 shows the computed Pareto-optimal solutions and a neural-network estimate of the Pareto-front. Point A in Fig. 4 represents the fin-shape, heat load (179.6 BTU/Hr.) and SOBTR (6.4 $^{\circ}$F) for the Pareto optimal solution corresponding to maximum heat load. Point B represents the fin shape, heat load (103.1 BTU/Hr.) and SOBTR (158.7 $^{\circ}$F) for the Pareto-optimal solution with the maximum SOBTR.

Figure 5 shows the variation of heat load as a function of the base temperature for the fins denoted as points A and B in Fig. 4. It is clear that fin B allows for a wide range of safe base temperatures about the nominal value of T_{base} = 320 $^{\circ}$F ($T_{base} - T_{ambient}$ = 200 $^{\circ}$F) but yields a lower heat load at the nominal value of base temperature. In contrast, fin A, yields a higher heat load at the nominal base temperature but has a smaller range of safe base temperature values. Figure 5 indicates that for a base temperature increase (over nominal) of about 10 $^{\circ}$F, film-boiling pervades the entire length of fin A. Figure 6 shows the shapes of fins A and B. The longer cylindrical base of fin B results in a larger temperature drop before the majority of the fin surface is encountered. Thus, up to a point, nucleate- and transition-boiling persist on the majority of the fin surface, even though the base temperature is much higher than the temperature at which film-boiling is initiated. However, at the nominal base temperature, the temperature drop in the base of the cylinder is larger than required for optimal operation and a larger portion of the fin is in a free-convection mode. This results in heat loads that are smaller than that obtained with fin A.

The multi-objective evolutionary method[4, 9] was found to be better suited to this fin optimization problem than response surface methodology and gradient based methods. This is because the discontinuity in the heat load as the base temperature is increased (Fig. 2) results in a discontinuity in the first objective function (Eq. 1) in design space. The high-heat-load Pareto optimal solutions lie in the vicinity of this discontinuity in the objective function. Thus computing the gradient or constructing standard response surfaces becomes problematic.

The fin optimization problem solved above has focused on obtaining the maximum heat load for a given value of SOBTR. Conceptually it is similar to aerodynamic shape optimization in the context of uncertain operating conditions. The next section focuses on design optimization in the presence of uncertainties in airfoil shape.

ROBUST AIRFOIL SHAPE OPTIMIZATION

The accuracy to which a component is manufactured depends on the available manufacturing technology and other factors such as manufacturing cost. Component shapes are also subject to change because of wear and tear. The performance, reliability and life expectancy of the component may depend critically on maintaining the shape of the component. Clearly there is a need to desensitize these aspects of the component to small (and perhaps large) changes in shape.

The following is an example that illustrates the use of mutiple-objective DE in desensitizing performance to changes in component shape. It consists of subsonic flow through a row of stator airfoils in an axial turbine. The flow is assumed to be inviscid and two-dimensional. Details regarding the grid generation and flow simulation procedures, and the airfoil parameterization method can be found elsewehere.[14-15] Although eight parameters were used to parameterize the airfoil, only two of them were varied during optimization. These two parameters have very little effect on the shape of the suction side of the airfoil. Their primary effect is on the shape of the pressure side of the airfoil. The first requirement is that the variance in pressure with small changes in airfoil shape is minimized. The second requirement is that the wedge angle at the trailing edge is maximized (this increases the thickness of the airfoil and thus its strength). These two requirements are to be met subject to the constraints that the required exit Mach number and flow turning angle are achieved. The two objective functions are defined as

$$\text{Minimize}: V = \sum_{n=1}^{n=nmax} \sum_{i=1}^{i=imax} (p_i - p_i^n)^2 \qquad (2)$$

$$\text{Minimize}: \theta = \theta_{ref} - \theta_w$$

In Eq. 2 imax is the number of grid points on the surface of the airfoil, nmax is the number of geometry perturbations used to compute the variance, p_i is the pressure at the ith point on the surface of the given geometry, and p_i^n is the surface pressure at the same point for the nth perturbation of this geometry. The quantity θ_{ref} is a reference angle and θ_w is the wedge angle. The manner in which the geometry perturbations are obtained depends on the probability density function assumed for the perturbations in the geometry. Egorov et al.[1] remark that a normal distribution is commonly observed for manufacturing tolerances. Here a simple approach is adopted; the perturbations are computed by perturbing one geometry variable at a time. Replacing this with normally distributed surface perturbations is straightforward.

The perturbed airfoil shapes as well as the base airfoil used in computing the objective function (Eq. 2) are obtained using the same airfoil parameterization scheme. This assumes that the geometry perturbations found in reality can be represented with the same number of geometric parameters that are used to represent the base airfoil. However, a finite number of geometry parameters can only yield approximate representations of the perturbations found in reality. Hence the approach computes approximations to the objective function of Eq. 2 (even when the sample size is large). Nevertheless the current approach has practical value. The set of perturbed airfoil shapes can be greatly enhanced by adding a perturbation function to the base airfoil shape. This function can be constructed with many more independent parameters governing its behavior than the number of parameters used to generate the base airfoil shape. This results in a very flexible perturbation function. Computing the variance with this extended set of airfoils is computationally expensive. Here we use the extended set only for assessment and not during optimization.

The DE search was conducted over 25 generations and with 10 parameter vectors. This required 780 two-dimensional airfoil simulations. Figure 7 shows the Pareto optimal solutions obtained at the end of this process. Normalized values of the two parameters that govern the shape of the airfoil are shown on the two axes. Points A and B on the estimate represent the minimum variance and maximum wedge angle

solutions, respectively. The computed optimal solutions exhibit a moderate amount of noise. A hybrid network consisting of 10 individual single-hidden-layer feed-forward networks was used to obtain an estimate of the Pareto optimal front using the training data from DE. The estimated Pareto front is also shown in Fig. 7. Continued evolution (10 additional generations requiring 300 flow simulations) only resulted in a small improvement in the computed solutions. On the other hand, the hybrid network estimate was obtained without requiring any additional simulations. Figure 8 shows training data and the estimate of the Pareto front in objective space. It is important to note that the estimating curve in this figure was obtained by selecting uniformly spaced points on the estimating curve in Fig. 7 and subsequently computing the flow over these selected shapes (and corresponding geometry perturbations).

Figure 9 shows the airfoils corresponding to the minimum variance and maximum wedge angle cases (points A and B in Fig. 7). The minimum variance case is a thinner airfoil whereas the maximum wedge angle case is thicker and thus stronger. Figure 10 shows the computed pressure distributions for the two airfoils. The minimum variance airfoil does not exhibit a suction side undershoot and the pressure is nearly constant in the last 75% of the axial chord. This is because sharp variations in pressure are generally sensitive to geometry variations and, are thus avoided in this airfoil. The estimate of the local standard deviation of pressure as a function of the axial location along the airfoil

$$\sigma_{local} = \left[\sum_{n=1}^{n=nmax} (p - p^n)^2 \right]^{1/2} \qquad (3)$$

for the two airfoils is shown in Figure 11. Thirty perturbations (nmax = 30) of the basic geometry and their corresponding flow fields were computed to determine σ_{local} in Eq. 3. The minimum variance airfoil yields a distribution that is significantly lower than that obtained with the airfoil with the maximum wedge angle. However, both these airfoils (and the other airfoils on the Pareto front) perform the same function of turning and accelerating the flow by a specified amount. The exit flow angle varied ±0.32% over the ten airfoils and, the exit Mach number varied± 0.04%.

In conclusion, simulation costs associated with robust optimal design will determine the rapidity with which this technology is assimilated into industrial practice. Since the number of simulations required for a particular design depends on the efficiency of the optimization algorithm utilized, improvements in algorithmic efficiency are critical. The introduction of surrogate models in the optimization procedure (Kriging models are used in Ref. 3 for reliability based design and neural networks are used in Ref. 16 to compute performance variability in robust optimal design) will certainly reduce design costs. The increased use of Pareto front estimators and hybrid approaches, for example evolutionary algorithms with embedded local search capability, will also serve to reduce design costs. The potential of increasing safety and, reducing maintenance costs makes robust optimal design a very exciting field of research.

REFERENCES

1. Egorov, I. N., Kretinin, G. V., and Leshchenko, I. A., “How to Execute Robust Design,” AIAA Paper No. 2002-5670, 9th AIAA/USAF/NASA/ISSMO Symposium on Multidisciplinary Analysis and Optimization, September 4-6, Atlanta, Georgia.

2. Koch, P. N., Wujek, B., Golovidov, O., “A Multi-Stage, Parallel Implementation of Probabilistic Design Optimization in an MDO Framework,” AIAA Paper No. 2000-4805, 8th AIAA/USAF/NASA/ISSMO Symposium on Multidisciplinary Analysis and Optimization, Long Beach, California.

3. Koch, P. N., Wujek, B., Golovidov, O., and Simpson, T. W., "Facilitating probabilistic multidisciplinary Design Optimization Using Kriging Approximation Models," 9th AIAA/USAF/NASA/ISSMO Symposium on Multidisciplinary Analysis and Optimization, September 4-6, Atlanta, Georgia.

4. Rai, M. M., " Single- and Multiple-Objective Optimization with Differential Evolution and Neural Networks", VKI Lecture Series on Optimization Methods & Tools for Multi-criteria/Multidisciplinary Design. Applications to Aeronautics and Turbomachinery, March 6 –10, 2006.

5. Deb, K., *Multi-Objective Optimization Using Evolutionary Algorithms*, Wiley, 2001.

6. Gonzalez, L., Whitney, E., Srinivas, K. and Periaux, J., "Multidisciplinary Aircraft Design and Optimization Using a Robust Evolutionary Technique with Variable fidelity Models", AIAA Paper No. 2004-4625, Tenth AIAA/ISSMO Multidisciplinary Analysis and Optimization Conference, Albany, New York, August 30 – Sep. 1, 2004.

7. Langer, H., Puehlhofer, T., and Baier, H., "A Multiobjective Evolutionary Algorithm with Integrated Response Surface Functionalities for Configuration Optimization with Discrete variables", AIAA Paper No. 2004-4326, Tenth AIAA/ISSMO Multidisciplinary Analysis and Optimization Conference, Albany, New York, August 30 – Sep. 1, 2004.

8. Chung, H. and Alonso, J., "Multiobjective Optimization Using Approximation Model Based Genetic Algorithms", AIAA Paper No. 2004-4325, Tenth AIAA/ISSMO Multidisciplinary Analysis and Optimization Conference, Albany, New York, August 30 – Sep. 1, 2004.

9. Rai, M. M., "Robust Optimal Design with Differential Evolution", Paper No. 2004-4588, Tenth AIAA/ISSMO Multidisciplinary Analysis and Optimization Conference, Albany, New York, August 30 – Sep. 1, 2004.

10. Price, K., and Storn, N., "Differential Evolution," *Dr. Dobb's Journal*, April 1997, pp. 18-24.

11. Haley, K. W., and Westwater, J. W., "Boiling Heat Transfer from Single Fins", *Proceedings of the Third International Heat Transfer Conference*, Volume 3, Page 245, 1966.

12. Westwater, J. W., Paper 1, "Heat Transfer – Fundamentals and Industrial Applications", *AICHE Symposium Series*, 69(131), Page 1,1973.

13. Rai, M. M., and Rangarajan, J., "Application of the Finite Element Method to Heat Conduction." Project Report, Department of Mechanical Engineering, Indian Institute of Technology, Madras, India, 1978.

14. Rai, M. M., "A Rapid Aerodynamic Design Procedure Based on Artificial Neural Networks," AIAA Paper No. 2001-0315, AIAA 39th Aerospace Sciences Meeting, Reno, Nevada, Jan. 8-11, 2001.

15. Rai, M. M., "Three-Dimensional Aerodynamic Design Using Artificial Neural Networks," AIAA Paper No. 2002-0987, AIAA 40th Aerospace Sciences Meeting, Reno, Nevada, Jan. 14-17, 2002.

16. Rai, M. M., "Robust Optimal Aerodynamic Design Using Evolutionary Methods and Neural Networks," AIAA Paper No. 2004-0778, AIAA 42nd Aerospace Sciences Meeting, Reno, Nevada, Jan. 5-8, 2004.

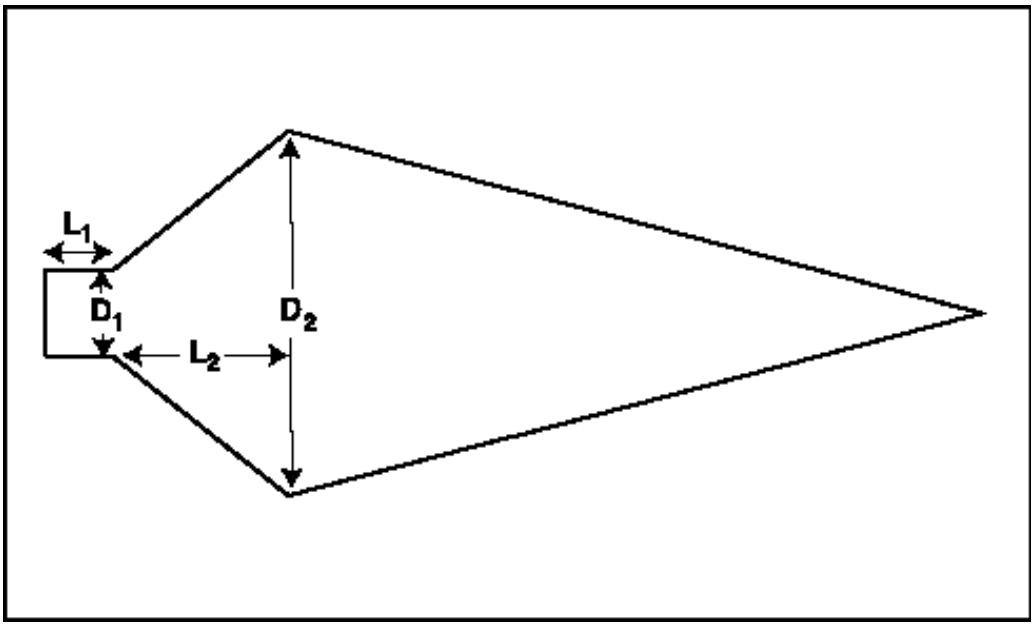

Fig. 1. Fin geometry and design variables.

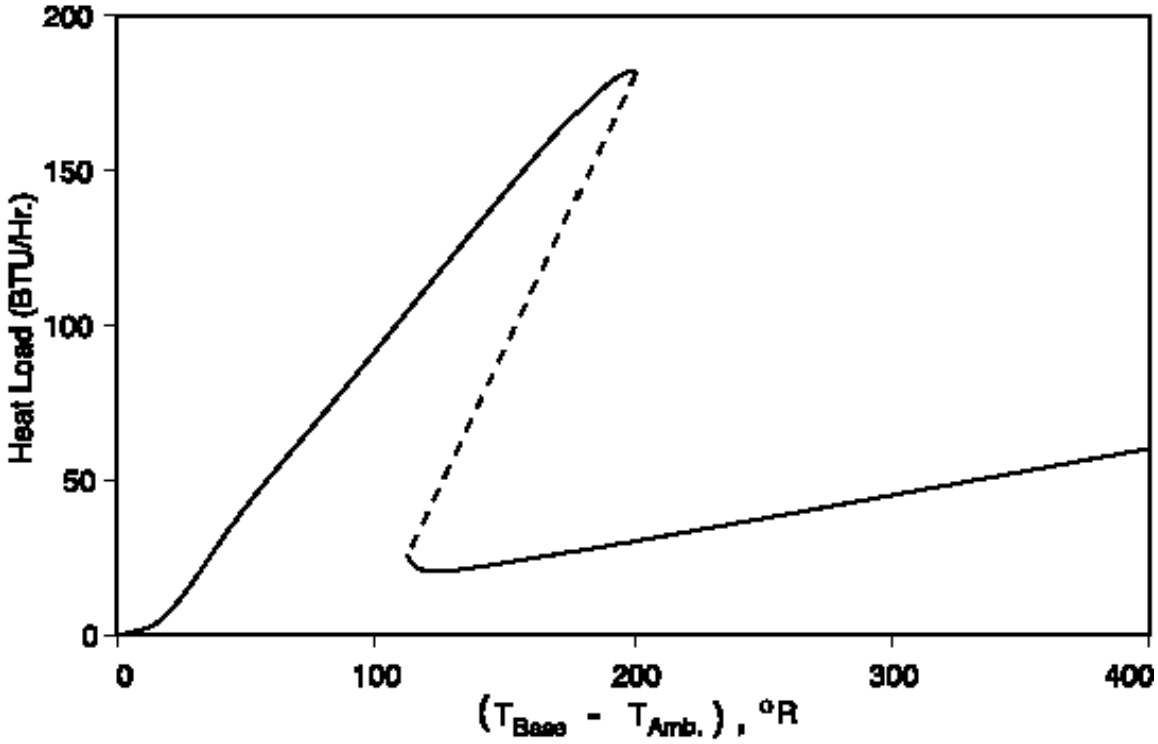

Fig. 2. Heat load at various base temperatures.

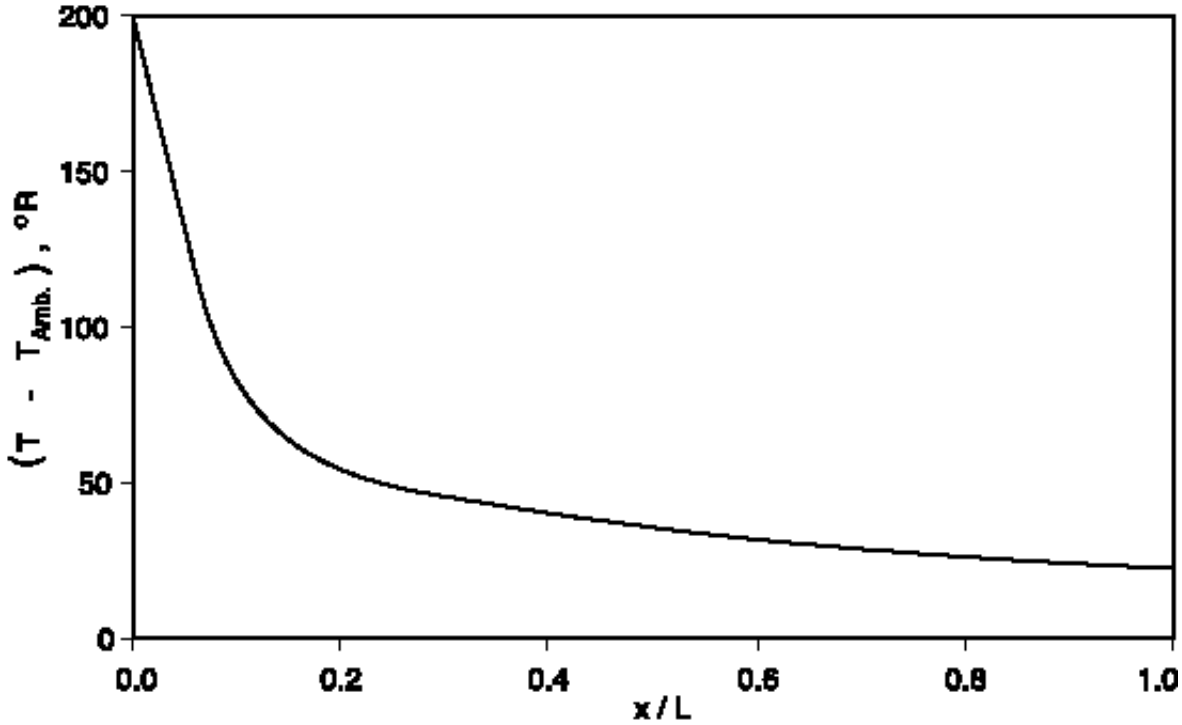

Fig. 3. Temperature variation along the axis of the fin.

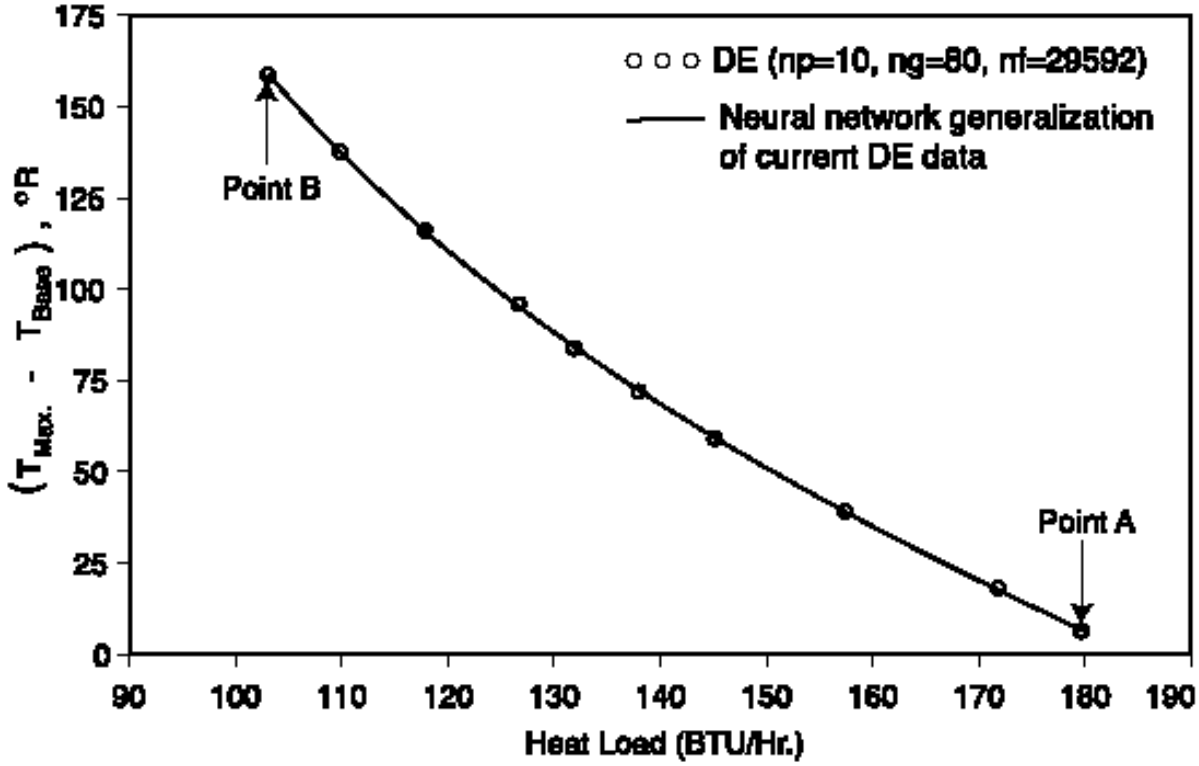

Fig. 4. Pareto optimal front in objective space for the fin showing the trade-off between heat load and safe operating base temperature range.

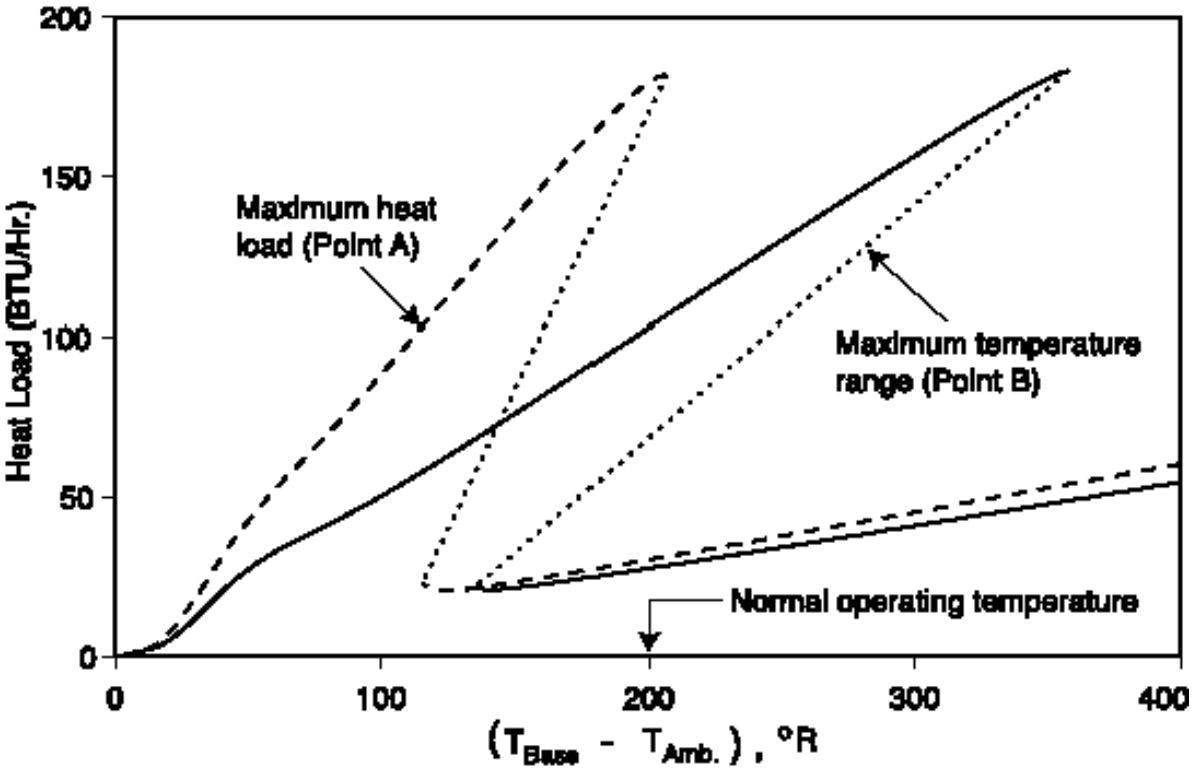

Fig. 5. Heat load as a function of base temperature for the maximum heat load and maximum SOBTR designs.

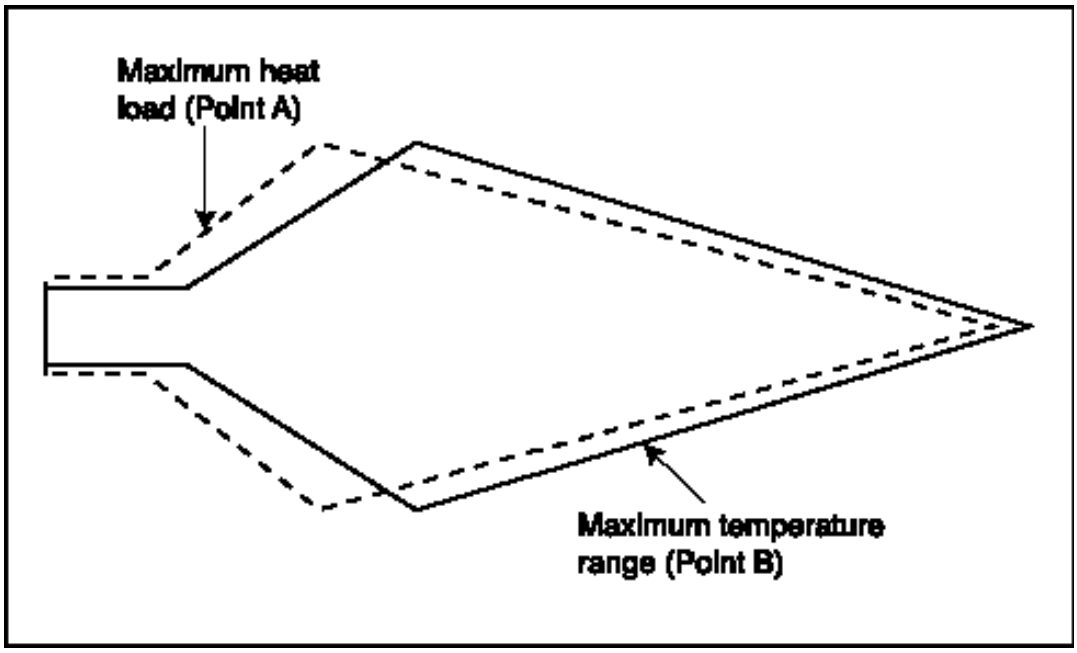

Fig. 6. Fin geometries for the maximum heat load and maximum SOBTR designs.

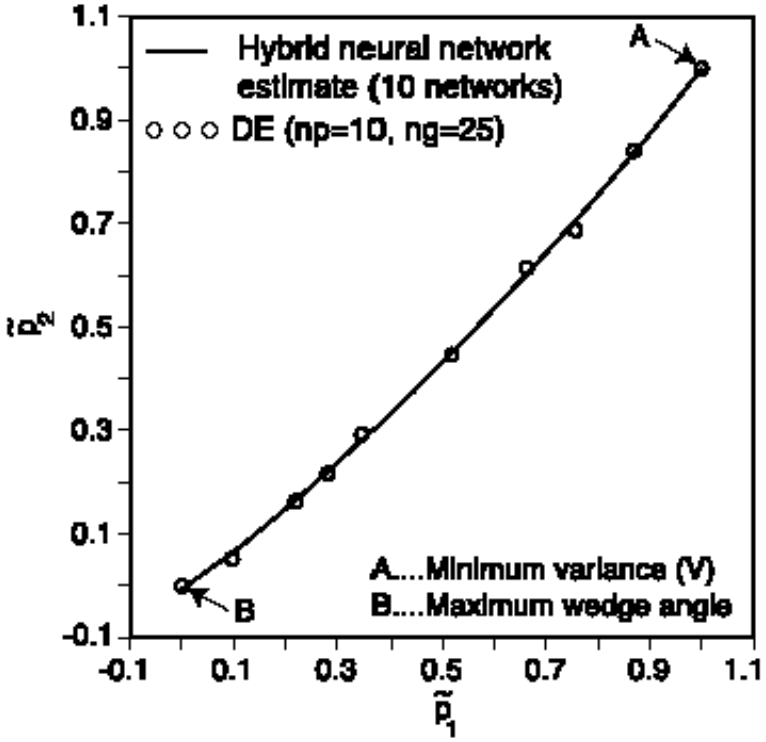

Fig. 7. Pareto optimal front in design space for the airfoil.

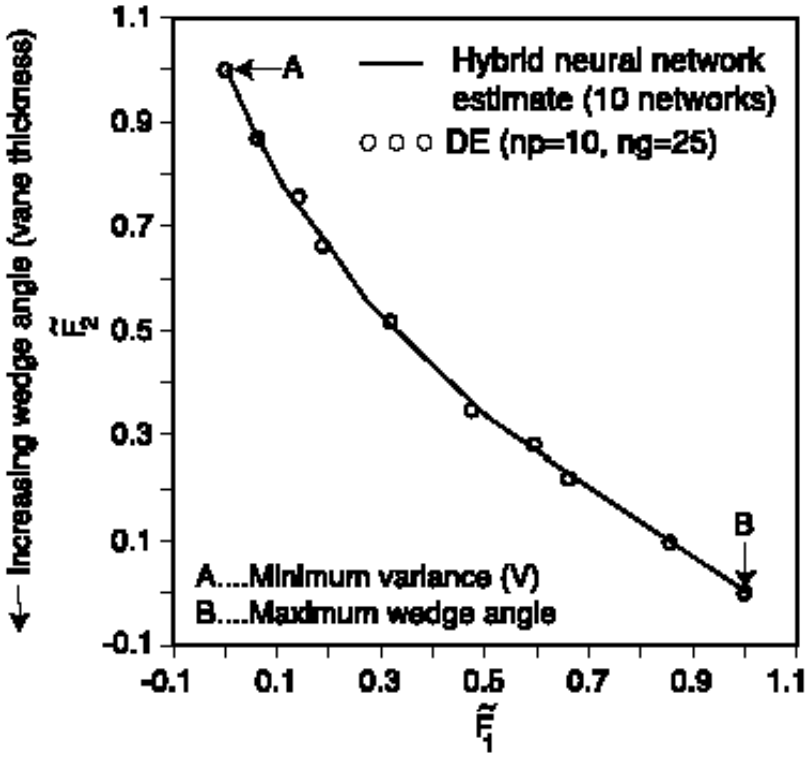

Fig. 8. Pareto optimal front in objective space for the airfoil.

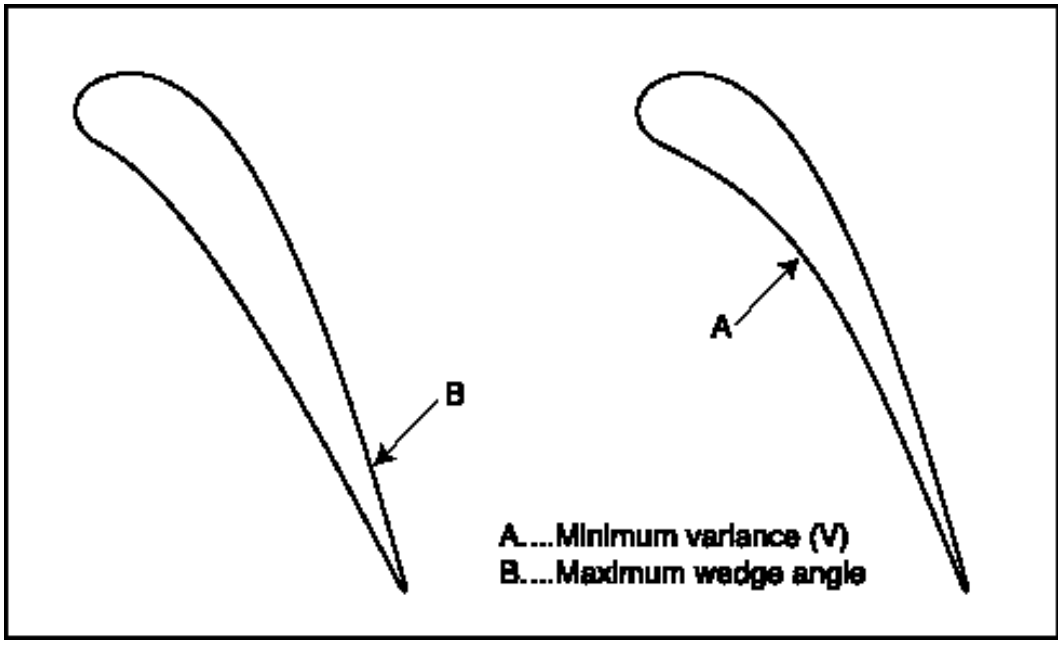

Fig. 9. Airfoil shapes corresponding to the minimum variance and maximum wedge angle cases.

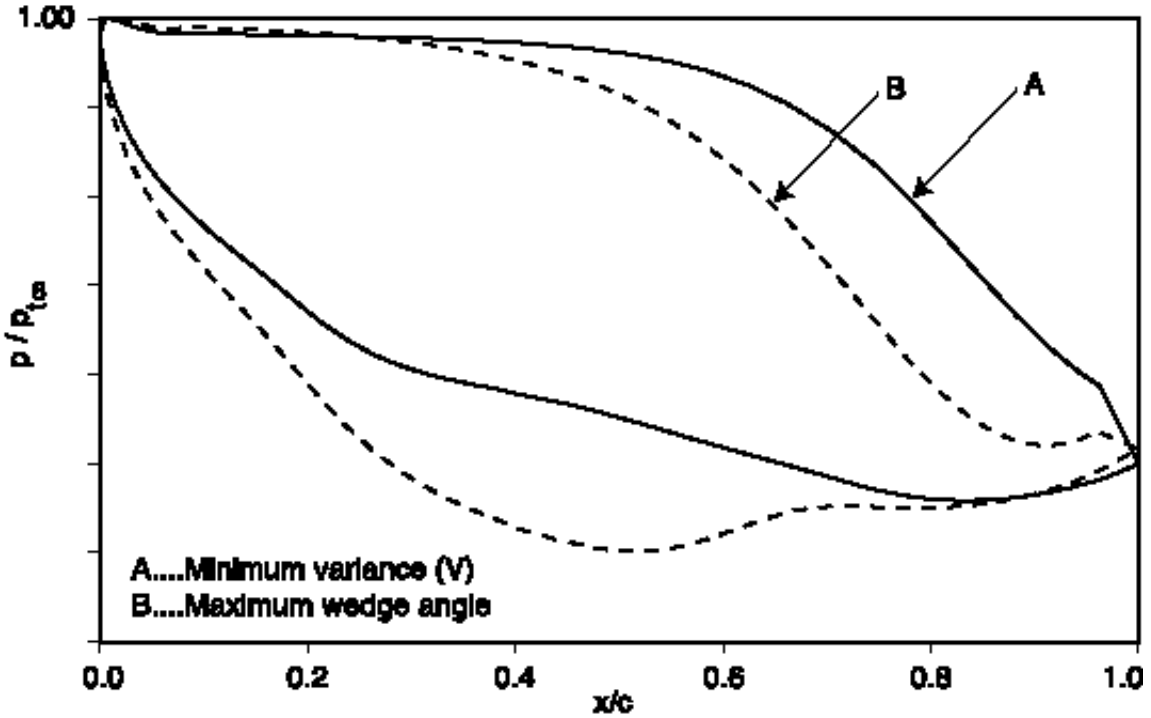

Fig. 10. Surface pressure distributions corresponding to the minimum variance and maximum wedge angle cases.

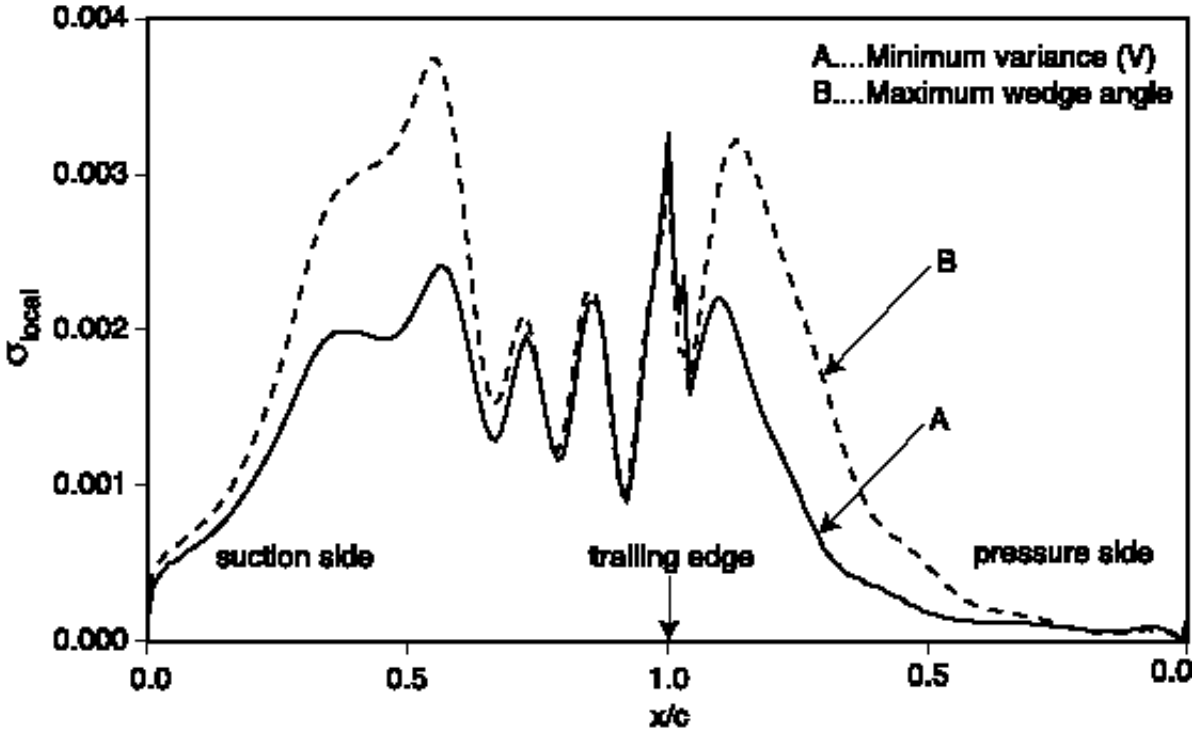

Fig. 11. Distribution of σ_{local} for the minimum variance and maximum wedge angle cases.